

HATS-59b,c: A TRANSITING HOT JUPITER AND A COLD MASSIVE GIANT PLANET AROUND A SUN-LIKE STAR [†]

P. SARKIS¹, TH. HENNING¹, J. D. HARTMAN², G. Á. BAKOS^{2,3*}, R. BRAHM^{4,5}, A. JORDÁN^{1,4,5}, D. BAYLISS⁶, L. MANCINI^{7,1,8}, N. ESPINOZA^{1,4,5}, M. RABUS^{1,4}, Z. CSUBRY², W. BHATTI², K. PENEV⁹, G. ZHOU¹⁰, J. BENTO¹¹, T. G. TAN¹², P. ARRIAGADA¹³, R. P. BUTLER¹⁴, J. D. CRANE¹⁴, S. SHECTMAN¹⁴, C. G. TINNEY^{15,16}, D. J. WRIGHT^{15,16}, B. ADDISON¹⁷, S. DURKAN¹⁸, V. SUC⁴, L. A. BUCHHAVE¹⁹, M. DE VAL-BORRO²⁰, J. LÁZÁR²¹, I. PAPP²¹, P. SÁRI²¹

Draft version May 16, 2018

ABSTRACT

We report the first discovery of a multi-planetary system by the HATSouth network, HATS-59b,c, a planetary system with an inner transiting hot Jupiter and an outer cold massive giant planet, which was detected via radial velocity. The inner transiting planet, HATS-59b, is on an eccentric orbit with $e = 0.129 \pm 0.049$, orbiting a $V = 13.951 \pm 0.030$ mag solar-like star ($M_{\star} = 1.038 \pm 0.039 M_{\odot}$ and $R_{\star} = 1.036 \pm 0.067 R_{\odot}$) with a period of 5.416081 ± 0.000016 days. The outer companion, HATS-59c is on a circular orbit with $m \sin i = 12.70 \pm 0.87 M_{\text{J}}$ and a period of 1422 ± 14 days. The inner planet has a mass of $0.806 \pm 0.069 M_{\text{J}}$ and a radius of $1.126 \pm 0.077 R_{\text{J}}$, yielding a density of $0.70 \pm 0.16 \text{ g cm}^{-3}$. Unlike most of the planetary systems that include only a single hot Jupiter, HATS-59b,c includes, in addition to the transiting hot Jupiter, a massive outer companion. The architecture of this system is valuable for understanding planet migration.

Subject headings: planetary systems — stars: individual (HATS-59) — techniques: spectroscopic, photometric

¹ Max Planck Institute for Astronomy, Heidelberg, Germany; sarkis@mpia.de

² Department of Astrophysical Sciences, Princeton University, NJ 08544, USA

³ MTA Distinguished Guest Fellow, Konkoly Observatory

⁴ Instituto de Astrofísica, Facultad de Física, Pontificia Universidad Católica de Chile, Av. Vicuña Mackenna 4860, 7820436 Macul, Santiago, Chile

⁵ Millennium Institute of Astrophysics, Av. Vicuña Mackenna 4860, 7820436 Macul, Santiago, Chile

⁶ Department of Physics, University of Warwick, Coventry CV4 7AL, UK

⁷ Department of Physics, University of Rome Tor Vergata, Via della Ricerca Scientifica 1, I-00133 Rome, Italy

⁸ INAF–Astrophysical Observatory of Turin, via Osservatorio 20, I-10025 Pino Torinese, Italy

⁹ Physics Department, University of Texas at Dallas, 800 W Campbell Rd. MS WT15, Richardson, TX 75080, USA

¹⁰ Harvard-Smithsonian Center for Astrophysics, Cambridge, MA 02138, USA

¹¹ Research School of Astronomy and Astrophysics, Australian National University, Canberra, ACT 2611, Australia

¹² Perth Exoplanet Survey Telescope, Perth, Australia

¹³ Department of Terrestrial Magnetism, Carnegie Institution for Science, Washington, DC 20015, USA

¹⁴ The Observatories of the Carnegie Institution for Science, 813 Santa Barbara St, Pasadena, CA 91101, USA

¹⁵ Australian Centre for Astrobiology, School of Physics, University of New South Wales, NSW 2052, Australia

¹⁶ Exoplanetary Science at UNSW, School of Physics, University of New South Wales, NSW 2052, Australia

¹⁷ Mississippi State University, Department of Physics & Astronomy, Hilbun Hall, Starkville, MS 39762, USA

¹⁸ Astrophysics Research Centre, Queens University, Belfast, Belfast, Northern Ireland, UK

¹⁹ DTU Space, National Space Institute, Technical University of Denmark, Elektrovej 328, DK-2800 Kgs. Lyngby, Denmark

²⁰ Astrochemistry Laboratory, Goddard Space Flight Center, NASA, 8800 Greenbelt Rd, Greenbelt, MD 20771, USA

²¹ Hungarian Astronomical Association, 1451 Budapest, Hungary

* Packard Fellow

[†] The HATSouth network is operated by a collaboration consisting of Princeton University (PU), the Max Planck Institute für Astronomie (MPIA), the Australian National Univer-

sity (ANU), and the Pontificia Universidad Católica de Chile (PUC). The station at Las Campanas Observatory (LCO) of the Carnegie Institute is operated by PU in conjunction with PUC, the station at the High Energy Spectroscopic Survey (H.E.S.S.) site is operated in conjunction with MPIA, and the station at Siding Spring Observatory (SSO) is operated jointly with ANU. This paper includes data gathered with 6.5 m Magellan Telescopes located at Las Campanas Observatory, Chile, and the MPG 2.2 m, the NTT, and the Euler 1.2 m telescopes at the ESO Observatory in La Silla. This paper uses observations obtained with facilities of the Las Cumbres Observatory Global Telescope. Based in part on observations made with the 3.9 m Anglo-Australian Telescope and the ANU 2.3 m Telescope both at SSO. Based in part on observations made with the facilities of the Las Cumbres Observatory Global Telescope, the Perth Exoplanet Survey Telescope, and the Nordic Optical Telescope.

1. INTRODUCTION

During the past decade, the number of exoplanets has increased steadily and by now more than 3500 exoplanets have been statistically validated. Exoplanets are very common and have a wide variety of properties (for a review check Winn & Fabrycky 2015), which offer a unique opportunity to constrain their formation and evolution (Mordasini et al. 2016; Jin & Mordasini 2018). Hot Jupiters, i.e. gas giant planets on short orbital periods, still pose many challenges for planet formation models. It is believed that such planets formed beyond the iceline, several au from the central star, and migrated inwards through interactions with the disk (e.g. Lin et al. 1996). However, disk migration predicts circular and aligned orbits (e.g. Goldreich & Tremaine 1980; Artymowicz 1993) and cannot explain the existence of several hot Jupiters that have been found on retrograde or misaligned orbits (for a review see Winn & Fabrycky 2015). Alternative scenarios have been thus proposed, which involve interactions with a third distant body or planet-planet scattering that can result in eccentric and misaligned orbits (Kozai 1962; Lidov 1962; Nagasawa et al. 2008; Li et al. 2014; Petrovich 2015).

One approach to put constraints on the different migration mechanisms is to measure the spin-orbit alignment via the Rossiter-McLaughlin effect (e.g., Queloz et al. 2000; Zhou et al. 2015). Another approach is to search for planetary or stellar companions at large separations, which could have influenced the dynamical evolution of the inner planet. Knutson et al. (2014) performed a long term radial velocity monitoring of 51 systems known to host a hot Jupiter, with the goal to detect further planetary companions. They estimated an occurrence rate of $51 \pm 10\%$ for companions with masses between $1-13M_J$ and orbital semi-major axes between 1-20 au. Ngo et al. (2015) presented the results on searching for stellar companions around 50 out of the 51 selected systems from Knutson et al. (2014) study. They corrected for survey incompleteness and reported a stellar companion fraction of $48 \pm 9\%$. Combining the results of both studies, Ngo et al. (2015) estimated that $72 \pm 16\%$ of hot Jupiters are part of multi-planet and/or multi-star systems.

In this work, we report the discovery of HATS-59b,c, the first multi-planet system detected by the HATSouth survey (Bakos et al. 2013). The star hosts an inner hot Jupiter detected via its transits and an outer cold massive giant planet detected via the radial velocity variations of the host star. The possibility of additional outer planetary companions to transiting hot Jupiter has been proposed, by e.g. Rabus et al. (2009) and in fact, there have been only a few transiting planets with an outer planetary companion for which a full orbit was detected via radial velocity, such as HAT-P-13b,c (Bakos et al. 2009), HAT-P-17b,c (Howard et al. 2012), Kepler-424b,c (Endl et al. 2014), WASP-41b,c (Neveu-VanMalle et al. 2016), WASP-47b,c (Hellier et al. 2012; Becker et al. 2015; Neveu-VanMalle et al. 2016), and WASP-53b,c (Triaud et al. 2017). Among all the systems with a transiting hot Jupiter known to have outer companions, HAT-P-13c and WASP-53b,c are the only massive planetary companions with a minimum mass greater than HATS-59c. The few detections of companions around transiting planets is due, to some extent, by the lack

of radial velocity follow-up observations. Hot Jupiters in multi-planet systems provide a unique opportunity to put observational constraints on migration models and also could be used to probe the tidal love number of the hot Jupiter (Buhler et al. 2016; Hardy et al. 2017), which in turn constrains the planetary interior structure (Batygin et al. 2009). Therefore, monitoring these systems is very interesting for planet formation and interior structure models.

The paper is structured as follows: in Section 2, we show the planetary signal detected by the HATSouth network and present the photometric and spectroscopic follow-up observations that allowed us to characterize the system. In Section 3, we derive the stellar parameters and jointly model the data to derive the planetary parameters. Our results are finally summarized in Section 4.

2. OBSERVATIONS

2.1. Photometry

2.1.1. Photometric detection

The star HATS-59 (Table 3) was observed by HATSouth instruments between UT 2010 January 19 and UT 2010 August 10 using the HS-1, HS-3, and HS-5 units at Las Campanas Observatory (LCO) in Chile, the H.E.S.S. site in Namibia, and Siding Springs Observatory (SSO) in Australia, respectively. A total of 3113, 4690 and 658 images of HATS-59 were obtained with the HS-1, HS-3 and HS-5 telescopes, respectively. The observations were obtained through a Sloan r filter with an exposure time of 240s. The data were reduced to trend-filtered light curves using the aperture photometry pipeline described by Penev et al. (2013) and making use of External Parameter Decorrelation (EPD; Bakos et al. 2010) and the Trend Filtering Algorithm (TFA; Kovács et al. 2005) to remove systematic variations. We searched for transits using the Box Least Squares (BLS; Kovács et al. 2002) fitting algorithm, and detected a $P = 5.4161$ day periodic transit signal in the light curve of HATS-59 (Figure 1; the data are available in Table 1). The per point RMS of the residual combined filtered HATSouth light curve (after subtracting the best-fit model transit) is 0.012 mag, which is typical for a star of this magnitude.

2.1.2. Photometric follow-up

In order to confirm that the transit signals detected in the discovery light curve are due to a transiting planet, we obtained photometric follow-up observations of three transit events. These light curves allow us to refine the ephemeris of the system and to determine precise parameters of the system. All the photometric data are provided in Table 1 and the follow-up light curves are shown in Figure 2 along with the best fit model and residuals.

An ingress was observed with the 0.3m Perth Exoplanet Telescope (PEST) on 3 March 2013, using the R_C filter. The photometric precision of the light curve was 5.0 mmag with a cadence of 130s. Another ingress was observed on 10 April 2013 using the Faulkes Telescope South (FTS), which is a fully automated telescope operated as part of the Las Cumbres Observatory Global Telescope (LCOGT; Brown et al. 2013). The transit was observed in the i -band filter achieving a photometric precision of 1.6 mmag with a cadence of 113s. An egress

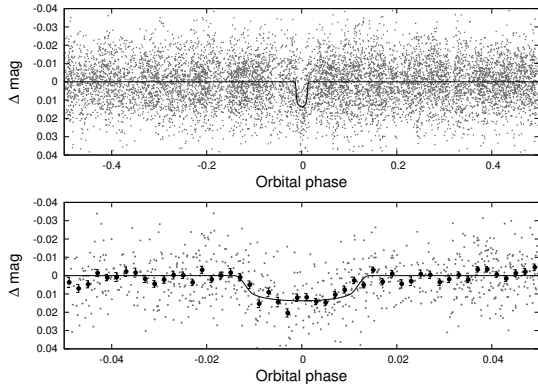


FIG. 1.— Unbinned instrumental r band light curve of HATS-59 folded with the period $P = 5.4160810$ days resulting from the global fit described in Section 3. The solid line shows the best-fit transit model (see Section 3). In the lower panel we zoom-in on the transit; the dark filled points here show the light curve binned in phase using a bin-size of 0.002.

was obtained on 21 December 2013 with the multiband imager GROND (Greiner et al. 2008), mounted on the 2.2 m telescope in La Silla Observatory, using four different filters (g , r , i , z). The light curve had a precision of 1.7 mmag in the g band, 1.0 mmag in r , 1.1 mmag in i , and 1.1 mmag in z , with a cadence of 168 s. The details of the data reduction for these facilities are described in Penev et al. (2013), Mohler-Fischer et al. (2013) and Zhou et al. (2014b).

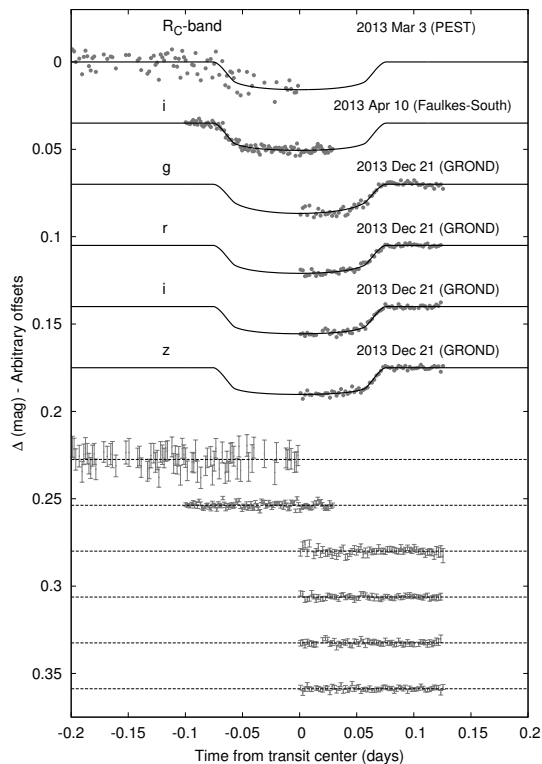


FIG. 2.— Unbinned follow-up transit light curve of HATS-59. The facilities and filters used, and the dates of each event are listed. Our best fit is shown by the solid lines. The residuals from the best fit model are shown below in the same order.

2.2. Spectroscopic Observations

HATS-59 was spectroscopically observed between April 2011 and March 2016 to confirm the planetary nature of the transit signals and to estimate the mass and therefore the density of the planet. Furthermore, the long radial velocity (RV) monitoring of the star allowed us to detect an outer companion with a longer orbital period than the transiting planet. We present the RV used to characterize the system in Figure 5 and provide the data in Table 2.

2.2.1. Reconnaissance Spectroscopy

Reconnaissance low-resolution spectroscopic follow-up observations are important to rule out various false positive scenarios, such as a primary giant star, or large RV variations indicating that the transiting object is itself a star. Reconnaissance spectroscopic observations were carried out with the WiFeS spectrograph (Dopita et al. 2007) on the ANU 2.3 m telescope. We obtained a single $R = 3000$ spectrum to estimate the stellar atmospheric parameters $T_{\text{eff},*}$, $[\text{Fe}/\text{H}]$, and $v \sin i$ and were used to confirm that the star is a dwarf. We also obtained 7 spectra with a higher resolution ($R = 7000$) to look for possible large RV variations at the $\sim 2 \text{ km s}^{-1}$ level. The spectra were extracted and reduced following Bayliss et al. (2013). Another reconnaissance spectrum was observed with the FIES spectrograph at the Nordic Optical Telescope (Telting et al. 2014), where it was reduced following Buchhave et al. (2010). We did not find large RV variations and thus ruled out the possibility that this system might be an eclipsing binary displaying a large radial velocity amplitude. We therefore proceeded with acquiring high precision RV observations to characterize the system.

2.2.2. High Precision Radial Velocities

We carried out an intensive RV follow-up campaign to measure, with high precision, the semi-amplitude of the RV variations due to the transiting planet. The RV observations showed variations in phase with the transit ephemeris of the interior planet. They, additionally, showed evidence for a large amplitude sinusoidal variation with a period of ~ 1400 days. We next describe the observations and the data reduction of all the spectrographs used in this analysis.

We obtained 9 spectra with CORALIE (Queloz et al. 2001), an echelle fibre-fed spectrograph mounted on the Euler 1.2 m in La Silla Observatory. We also obtained 5 spectra with the Planet Finder Spectrograph (PFS, Crane et al. 2010) on the Magellan Clay 6.5 m in Las Campanas Observatory and 7 spectra with CYCLOPS on the 3.9 m Anglo-Australian Telescope. Most of the spectra used in this analysis, most importantly for the discovery of the second outer companion, were obtained with FEROS on the MPG 2.2 m (Kaufer & Pasquini 1998) in La Silla Observatory. We observed a total of 24 spectra with FEROS, which is a high resolution echelle spectrograph (Kaufer & Pasquini 1998). All the spectra acquired with FEROS and CORALIE were reduced, extracted, and analysed using the CERES pipeline (Brahm et al. 2017a). For the data reduction of PFS spectra, we obtained a template spectrum by using the $0''.5$ slit, which was then used as reference for computing the radial ve-

TABLE 1
DIFFERENTIAL PHOTOMETRY OF HATS-59

BJD (2 400 000+)	Mag ^a	σ_{Mag}	Mag(orig) ^b	Filter	Instrument
55372.26299	-0.01448	0.00725	...	<i>r</i>	HS/G563.1
55274.77568	0.01224	0.00650	...	<i>r</i>	HS/G563.1
55296.44071	0.01384	0.00668	...	<i>r</i>	HS/G563.1
55274.77891	-0.01225	0.00628	...	<i>r</i>	HS/G563.1
55296.44428	-0.00169	0.00659	...	<i>r</i>	HS/G563.1
55274.78240	-0.01307	0.00627	...	<i>r</i>	HS/G563.1
55296.44754	-0.00042	0.00652	...	<i>r</i>	HS/G563.1
55274.78561	0.00435	0.00643	...	<i>r</i>	HS/G563.1
55296.45080	-0.00521	0.00660	...	<i>r</i>	HS/G563.1
55372.27744	0.00356	0.00771	...	<i>r</i>	HS/G563.1

NOTE. — This table is available in a machine-readable form in the online journal. A portion is shown here for guidance regarding its form and content. The data are also available on the HATSouth website at <http://www.hatsouth.org>.

^a The out-of-transit level has been subtracted. For the HATSouth light curve (rows with “HS” in the Instrument column), these magnitudes have been detrended using the EPD and TFA procedures prior to fitting a transit model to the light curve. For the follow-up light curves (rows with an Instrument other than “HS”) these magnitudes have been detrended with the EPD procedure, carried out simultaneously with the transit fit.

^b Raw magnitude values without application of the EPD procedure. This is only reported for the follow-up light curve.

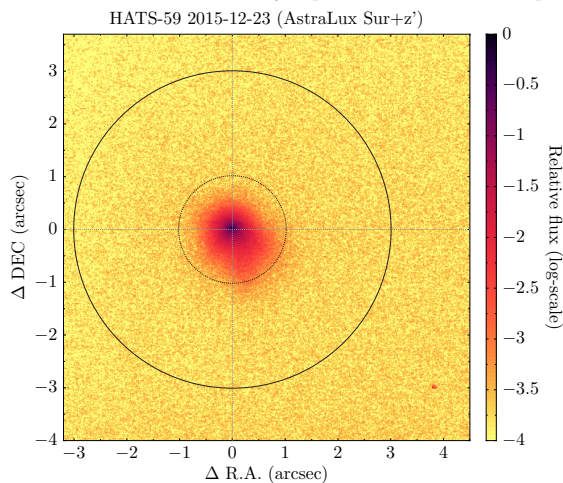


FIG. 3.— Astralux Sur lucky image of HATS-59 using z' . Circles of $1''$ and $3''$ radii are shown. No neighboring companion is detected within $2''$.

locities at different epochs by obtaining spectra with an I2-cell. The spectra that were acquired with the I2-cell were processed as described in Butler et al. (1996). Details on the data reduction and analysis are described in previous HATSouth discovery papers, e.g. Jordán et al. (2014); Zhou et al. (2014a); Hartman et al. (2015). For details of the data reduction of CYCLOPS spectra, see Penev et al. (2013).

2.3. Lucky Imaging

High spatial resolution imaging were obtained as part of the follow-up campaign using the Astralux Sur camera (Hippler et al. 2009) on the New Technology Telescope (NTT), at La Silla Observatory in Chile. These observations are useful to identify close stellar companions that could affect the transit depth. Lucky imaging observations were obtained on December 23, 2015 using the SDSS z' filter and reduced following Espinoza et al. (2016) but we used instead the plate scale derived in

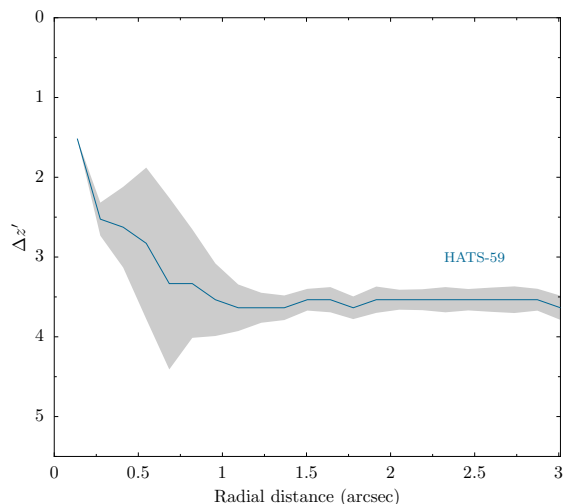


FIG. 4.— Contrast curve for of HATS-59 using the Astralux Sur z' observations. Gray bands show the uncertainty given by the scatter in the contrast in the azimuthal direction at a given radius.

Janson et al. (2017) of 15.2 mas/pixel , which is a better estimate than the one estimated in our previous work. Figure 3 shows the final reduced image and Figure 4 shows the contrast curve, where no resolved companion is detected within $2''$.

3. ANALYSIS

3.1. Properties of the Parent Star

It is important to characterize the host star in order to measure precise planetary parameters. We used ZASPE (Brahm et al. 2017b) to get an initial estimate of the atmospheric parameters ($T_{\text{eff}\star}$ [Fe/H] $v \sin i$, and $\log g_{\star}$). The parameters were determined using the FEROS spectra, which were co-added to obtain a high signal-to-noise ratio spectrum. ZASPE determines the stellar parameters via least-squares minimization against a grid of synthetic spectra in the spectral regions most sensitive to

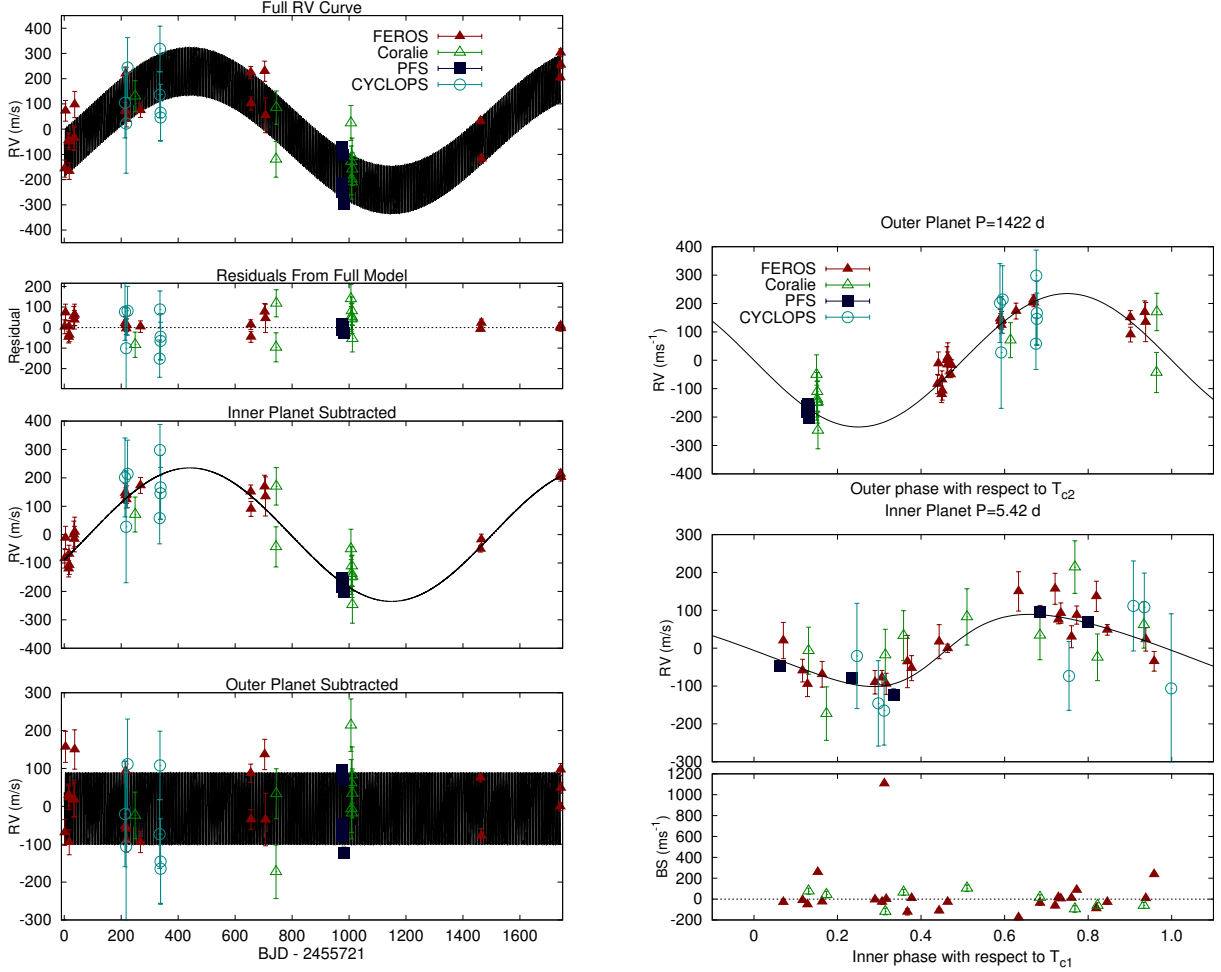


FIG. 5.— *Top left:* High-precision RV measurements from MPG 2.2 m/FEROS, Euler 1.2 m/Coralie, Magellan 6.5 m/PFS, and AAT-3.9m/CYCLOPS, together with our best-fit two-planet orbit model, plotted as a function of time. The center-of-mass velocity has been subtracted. The error bars include the jitter which is varied independently for each instrument in the fit. *Left, second panel:* RV $O-C$ residuals from the two planet model, plotted as a function of time. *Left, third panel:* RV residuals after subtracting only the model variation due to the inner planet, plotted as a function of time. *Left, bottom panel:* RV residuals after subtracting only the model variation due to the outer planet, plotted as a function of time. *Top right:* RV residuals after subtracting only the model variation due to the inner planet, plotted as a function of phase of the outer planet. Here zero phase corresponds to the time of inferior conjunction for the outer planet. *Right, second panel:* RV residuals after subtracting only the model variation due to the outer planet, plotted as a function of phase of the inner planet. *Right, bottom panel:* Spectral line bisector spans (BSs) plotted as a function of phase of the inner planet. Note the different vertical scales of all of the panels.

changes in the parameters (5000 \AA and 6000 \AA).

We then followed Sozzetti et al. (2007) to determine the fundamental stellar parameters (M_* , R_* , L_* , age, etc.). In particular, we used the stellar density ρ_* determined from the photometric light curve, combined with the $T_{\text{eff}*}$ and $[\text{Fe}/\text{H}]$ measurements, to characterize the host star. The parameters were obtained by combining the spectroscopic and photometric parameters with the Yonsei-Yale stellar evolution models (Y^2 ; Yi et al. 2001). This provided a revised estimate of $\log g_*$, which was fixed in a second iteration of ZASPE that returned the final values of the stellar parameters.

We find that the star HATS-59 has a mass of $1.038 \pm 0.039 M_\odot$, a radius of $1.036 \pm 0.067 R_\odot$, and is at a reddening-corrected distance of $630 \pm 43 \text{ pc}$. The distance estimated using isochrone fitting is in agreement with the distance estimated using Gaia data. Figure 6 shows the location of the star on the $T_{\text{eff}*}-\rho_*$ diagram and the final adopted stellar parameters are listed in Table 3.

3.2. Excluding Blend Scenarios

In order to rule out the possibility that HATS-59 is a blended stellar eclipsing binary system, we carried out a blend analysis of the photometric data following Hartman et al. (2012). We find that although blended stellar eclipsing binary models can be found which fit the available photometric data, these models would produce obviously composite spectroscopic cross-correlation functions (CCFs) that are inconsistent with the observed CCFs. For example, in all cases the spectral line bisector spans (BSs) computed from the simulated CCFs have scatter in excess of 10 km s^{-1} , whereas, excluding one outlier, the scatter of the measured FEROS BSs is $\sim 100 \text{ m s}^{-1}$. Similarly the RVs of the simulated CCFs are in excess of 500 m s^{-1} , whereas the observed FEROS RVs have a scatter of 130 m s^{-1} (dominated by the planetary signals). We conclude that HATS-59 is not a blended stellar eclipsing binary, and is instead a transiting planet sys-

TABLE 2
RELATIVE RADIAL VELOCITIES AND BISECTOR SPAN MEASUREMENTS OF
HATS-59.

BJD (2 450 000+)	RV ^a (m s ⁻¹)	σ_{RV}^b (m s ⁻¹)	BS (m s ⁻¹)	σ_{BS}	Phase	Instrument
5722.48192	-156.41	34.00	-25.0	16.0	0.163	FEROS
5725.50346	72.59	41.00	-64.0	19.0	0.721	FEROS
5736.54834	-43.41	29.00	10.0	14.0	0.760	FEROS
5737.51083	-49.41	31.00	7.0	15.0	0.938	FEROS
5738.54029	-166.41	33.00	-52.0	16.0	0.128	FEROS
5754.47565	-35.41	48.00	-29.0	21.0	0.070	FEROS
5756.49554	-36.41	45.00	-111.0	20.0	0.443	FEROS
5757.52534	97.59	52.00	-177.0	21.0	0.633	FEROS
5934.15946	104.14	109.00	0.246	CYCLOPS
5934.86914	72.59	33.00	8.0	16.0	0.377	FEROS
5936.80355	219.59	27.00	4.0	13.0	0.735	FEROS
5938.23445	22.14	177.00	0.999	CYCLOPS
5938.87128	69.59	30.00	-11.0	14.0	0.116	FEROS
5939.81042	39.59	31.00	-6.0	15.0	0.290	FEROS
5943.16020	244.14	82.00	0.908	CYCLOPS
5969.77597	130.39	36.00	-61.0	26.0	0.822	Coralie
5988.70024	74.59	28.00	0.0	14.0	0.317	FEROS
6056.06292	136.14	29.00	0.754	CYCLOPS
6057.03928	318.14	27.00	0.934	CYCLOPS
6059.00663	65.14	73.00	0.298	CYCLOPS
6059.08191	46.14	30.00	0.312	CYCLOPS
6375.71072	224.59	24.00	87.0	12.0	0.773	FEROS
6376.71477	101.59	26.00	237.0	13.0	0.958	FEROS
6377.76897	258.0	12.0	0.153	FEROS
6378.63214	1107.0	13.0	0.312	FEROS
6424.70951	229.59	40.00	-90.0	18.0	0.820	FEROS
6427.67642	54.59	69.00	-123.0	30.0	0.367	FEROS
6464.53773	-119.61	50.00	43.0	32.0	0.173	Coralie
6465.53888	85.39	43.00	65.0	29.0	0.358	Coralie
6694.77700	-71.73	6.28	0.684	PFS
6696.82969	-214.95	4.90	0.063	PFS
6697.75879	-248.73	4.86	0.234	PFS
6700.82214	-101.76	5.72	0.800	PFS
6703.71677	-296.25	8.71	0.334	PFS
6727.73071	24.39	48.00	-95.0	32.0	0.768	Coralie
6728.62473	-128.61	36.00	-61.0	29.0	0.933	Coralie
6729.69322	-197.61	37.00	76.0	29.0	0.131	Coralie
6730.68884	-209.61	46.00	-119.0	32.0	0.314	Coralie
6731.74803	-109.61	55.00	104.0	32.0	0.510	Coralie
6732.69422	-158.61	41.00	15.0	26.0	0.685	Coralie
7182.46643	32.59	11.00	16.0	15.0	0.729	FEROS
7185.59484	-117.41	19.00	-27.0	25.0	0.306	FEROS
7462.66518	204.59	11.00	-28.0	16.0	0.464	FEROS
7463.86306	302.59	16.00	-37.0	21.0	0.685	FEROS
7464.73538	254.59	14.00	-29.0	19.0	0.846	FEROS

^a Relative RVs, with γ_{RV} subtracted.

^b Internal errors excluding the component of astrophysical/instrumental jitter considered in Section 3.

tem.

3.3. Global Modeling of the Data

To measure the orbital and physical properties of the planets, we modeled all the photometric data (the HATSouth and follow-up photometric data) and the high-precision RV measurements following Pál et al. (2008) Bakos et al. (2010) and Hartman et al. (2012).

All the photometric light curves were modeled using the Mandel & Agol (2002) transit models with fixed quadratic limb darkening coefficients taken from Claret (2004). For the HATSouth discovery photometric light curves, we also considered a dilution factor for the transit depth that accounts for possible blends from neighboring stars and possible over-correction introduced by the trend filtering algorithm (TFA; removes trends shared with other stars; Bakos et al. 2010; Kovács et al. 2005). As for the photometric follow-up light curves, the sys-

tematic trends were corrected by including a quadratic trend to the transit model. We also added a linear trend, with up to three parameters, to reconstruct the shape of the PSF. This trend compensates for changes in the PSF during the observations, which could be due to poor guiding, non-photometric conditions, or changes in the seeing during the transit observations.

We fit the RVs, taken with different spectrographs, with a Keplerian orbit allowing the zero-point and the RV jitter, for each instrument, to vary independently in the fit. Our RVs support the existence of a second planet on top of the transiting one, and therefore models with two planets were considered in the modelling. We considered four different scenarios where one or both of the planets had a fixed circular orbit, or was allowed to have non-zero eccentricity. To choose between the different scenarios, we estimated the Bayesian evidence for

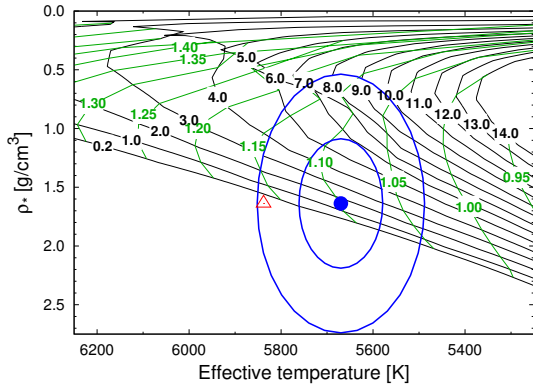


FIG. 6.— Model isochrones (black solid lines) from Yi et al. (2001) for the measured metallicity of HATS-59. The age of each isochrone in Gyr is labeled in black font. We also show evolutionary tracks for stars of fixed mass (dashed green lines) with the mass of each tracked labeled in solar mass units in green font. The adopted values of $T_{\text{eff}\star}$ and ρ_{\star} are shown using the filled blue circle together with their 1σ and 2σ confidence ellipsoids (blue lines). The initial values of $T_{\text{eff}\star}$ and ρ_{\star} from the first ZASPE and light curve analysis are represented with the red open triangle.

each model following Weinberg et al. (2013), and then adopted the model with the highest evidence, which we find to be a model in which the interior transiting planet has a non-zero eccentricity, while the exterior planet has a circular orbit. The evidence for this model is a modest factor of 2.4 times greater than the evidence for the model in which both planets are assumed to have circular orbits, 7 times greater than the model in which the interior planet is circular and the exterior planet has an eccentric orbit, and 19 times greater than the model in which both planets have non-zero eccentricities.

This analysis makes use of a differential evolution Markov Chain Monte Carlo procedure (DEMCMC; ter Braak 2006) to estimate the posterior parameter distributions, which we use to determine the median parameter values and their 1σ uncertainties. We find that the transiting planet HATS-59b has a mass of $0.806 \pm 0.069 M_{\text{J}}$, a radius of $1.126 \pm 0.077 R_{\text{J}}$, and a non-zero eccentricity of $e = 0.129 \pm 0.049$. For the second planet, which we dub HATS-59c, we find that it is well fit by a circular Keplerian orbit with $P = 1422 \pm 14$ days, $K = 224 \pm 14 \text{ m s}^{-1}$, implying a minimum mass for the companion of $m \sin i = 12.70 \pm 0.87 M_{\text{J}}$, where i is the orbital inclination of HATS-59c.

4. DISCUSSION

We present the discovery of HATS-59, the first multi-planet system detected by the HATSouth survey. The inner planet, HATS-59b, is a transiting hot Jupiter on an eccentric orbit, completing one revolution every ≈ 5 days. The outer planet, HATS-59c, is a cold massive giant planet on a circular orbit with a period of 1422 days.

4.1. Possible Formation Scenarios of HATS-59b,c

The architecture of HATS-59b,c poses a challenge for planet formation and migration scenarios. Can core accretion explain the presence of a hot Jupiter and a massive gas giant in the same system? Schlaufman (2018) found that planets with $M > 10 M_{\text{J}}$ do not preferentially orbit metal-rich solar-like stars, suggesting that these objects most likely did not form via core accretion but via

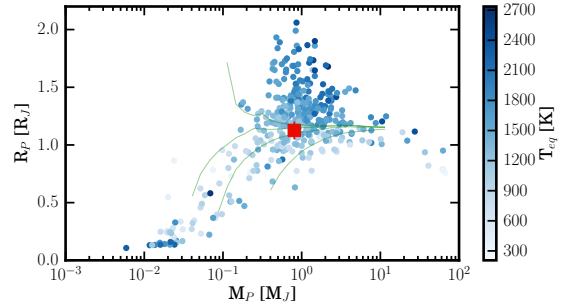


FIG. 7.— Mass - Radius diagram for the full population of well characterized transiting planets colour coded by their equilibrium temperature. HATS-59b is shown in red. The Fortney et al. (2007) models of planetary structure are also plotted as green lines. The four models correspond to gaseous planets with $a=0.045$ AU, age=4.3 Gyr, and core masses of 0, 25, 50, and $100 M_{\oplus}$.

gravitational instability. The architecture of HATS-59b,c hence suggests that both core accretion and gravitational instability could have occurred in the same system, which was also previously suggested by Triaud et al. (2017) for WASP-53bc and WASP-81bc.

The current water iceline is around 2.92 au, suggesting that both HATS-59b and HATS-59c formed beyond the iceline and then migrated inwards to their present locations. The presence of HATS-59c, a massive companion close to the deuterium burning limit (Mollière & Mordasini 2012), could have scattered HATS-59b inwards resulting in its present eccentric orbit. Due to its mass, type-II migration is reduced even below the viscous limit for HATS-59c (Baruteau et al. 2014), resulting in only little inward migration, potentially explaining its long period.

4.2. Transit Timing Variations

Variations in the times of transits can be attributed to the presence of a secondary planet in the system (e.g. Agol et al. 2005; Mancini et al. 2016; Almenara et al. 2018). The maximum transit variation expected for the inner planet is on the order of 10^{-10} s, undetectable with current instruments. However, this depends on the mutual inclination between the inner and outer planet.

4.3. The Inner Transiting Planet HATS-59b

In Figure 7, we plot the masses and radii of all the transiting exoplanets having these parameters measured with a precision better than 20%. HATS-59b lies in a densely populated region of the parameter space, where numerous non inflated giant planets with similar properties have been detected. In terms of structure, HATS-59b is similar to HAT-P-29 b ($M_p = 0.78 M_{\text{J}}$, $R_p = 1.11 R_{\text{J}}$, and $P = 5.7$ days; Buchhave et al. 2011); and K2-115 b, ($M_p = 0.84 M_{\text{J}}$, $R_p = 1.12 R_{\text{J}}$, and $P = 20.3$ days; Shporer et al. 2017), however with a significantly shorter period.

We compare the mass and radius of HATS-59b to the theoretical models of Fortney et al. (2007), for a hydrogen-helium dominated planets with different core masses, at a distance of 0.045 AU, and an age of 4.3 Gyr. We find that its composition is consistent with a gas-dominated planet with a core mass $M_c < 25 M_{\oplus}$. However, these models assume that all the solid material is located inside the core. According to Thorngrén et al.

TABLE 3
STELLAR PARAMETERS FOR HATS-59

Parameter	Value	Source
Identifying Information		
R.A. (h:m:s)	11 ^h 21 ^m 18.00s	2MASS
Dec. (d:m:s)	−22°23′17.4″	2MASS
R.A.p.m. (mas/yr)	−24.16 ± 0.047	Gaia DR2
Dec.p.m. (mas/yr)	0.92 ± 0.03	Gaia DR2
Parallax (mas)	1.52 ± 0.03	Gaia DR2
GSC ID	GSC 6090-00133	GSC
2MASS ID	2MASS 11211786-2223174	2MASS
Spectroscopic properties		
$T_{\text{eff}\star}$ (K)	5670 ± 91	ZASPE ^a
[Fe/H]	0.180 ± 0.064	ZASPE
$v \sin i$ (km s ^{−1})	2.80 ± 0.61	ZASPE
γ_{RV} (m s ^{−1})	−10887 ± 11	FEROS
Photometric properties		
B (mag)	14.727 ± 0.020	APASS
V (mag)	13.951 ± 0.030	APASS
g (mag)	14.286 ± 0.030	APASS
r (mag)	13.725 ± 0.030	APASS
i (mag)	13.551 ± 0.040	APASS
J (mag)	12.590 ± 0.024	2MASS
H (mag)	12.299 ± 0.030	2MASS
K_s (mag)	12.238 ± 0.030	2MASS
G (mag)	13.785	Gaia DR2
Derived properties		
M_\star (M_\odot)	1.038 ± 0.039	Y ² + ρ_\star +ZASPE ^b
R_\star (R_\odot)	1.036 ± 0.067	Y ² + ρ_\star +ZASPE
$\log g_\star$ (cgs)	4.422 ± 0.053	Y ² + ρ_\star +ZASPE
ρ_\star (g cm ^{−3}) ^c	1.59 ± 0.54	Light curves
ρ_\star (g cm ^{−3}) ^c	1.31 ± 0.24	Y ² +Light curves+ZASPE
L_\star (L_\odot)	0.99 ± 0.16	Y ² + ρ_\star +ZASPE
M_V (mag)	4.86 ± 0.19	Y ² + ρ_\star +ZASPE
M_K (mag,ESO)	3.24 ± 0.14	Y ² + ρ_\star +ZASPE
Age (Gyr)	4.3 ± 2.3	Y ² + ρ_\star +ZASPE
A_V (mag) ^d	0.091 ± 0.074	Y ² + ρ_\star +ZASPE
Distance (pc)	654 ± 14	Gaia DR2

^a ZASPE = “Zonal Atmospheric Stellar Parameter Estimator” method for the analysis of high-resolution spectra (Brahm et al. 2017b) applied to the FEROS spectra of HATS-59. These parameters rely primarily on ZASPE, but have a small dependence also on the iterative analysis incorporating the isochrone search and global modeling of the data, as described in the text.

^b Isochrones+ ρ_\star +ZASPE = Based on the Y² isochrones (Yi et al. 2001), the stellar density used as a luminosity indicator, and the ZASPE results.

^c We list two values for ρ_\star . The first value is determined from the global fit to the light curves and RV data, without imposing a constraint that the parameters match the stellar evolution models. The second value results from restricting the posterior distribution to combinations of ρ_\star + $T_{\text{eff}\star}$ + [Fe/H] that match to a Y² stellar model.

^d Total V band extinction to the star determined by comparing the catalog broad-band photometry listed in the table to the expected magnitudes from the Isochrones+ ρ_\star +ZASPE model for the star. We use the Cardelli et al. (1989) extinction law.

(2016), HATS-59b could have a larger amount of heavy elements in its interior ($\sim 50 M_\oplus$) if they are predominantly mixed in the gaseous envelope.

4.3.1. Possible Migration Scenarios of HATS-59b

Hot Jupiters are thought to form beyond the iceline and migrate inwards via disk or high eccentricity migration, where the latter requires an outer planetary or stellar companion. Observations of the projected spin-orbit angle via the Rossiter-McLaughlin (RM) effect provides an approach to distinguish between these migration scenarios. Disk migration predicts circular and aligned orbits, whereas the high eccentricity migration can pro-

duce a broad range of obliquities, depending mostly on the scattering mechanism and on the effectiveness of tidal interactions at damping obliquities.

The amplitude of the RM effect scales with $v \sin i$, the projected rotational velocity of the star. We predict an RM amplitude of 23 – 36 m s^{−1} for $v \sin i = 2.2 - 3.4$ km s^{−1}. Measuring the RM amplitude for this faint star ($V = 13.951 \pm 0.030$ mag), is challenging but plausible using HIRES (Vogt et al. 1994; Wang et al. 2018) on the Keck telescope or with the new high-resolution spectrograph, ESPRESSO (Pepe et al. 2014) at the Very Large Telescope.

Disk migration predicts that planets can migrate

TABLE 4
PARAMETERS FOR THE PLANETS HATS-59B,C.

Parameter	HATS-59b Value ^a	HATS-59c Value ^a
Light curve parameters		
P (days)	5.416081 ± 0.000016	1422 ± 14
T_c (BJD) ^b	$2456620.66527 \pm 0.00052$	2456521 ± 11
T_{14} (days) ^b	0.1497 ± 0.0017	0.957 ± 0.054
$T_{12} = T_{34}$ (days) ^b	0.0186 ± 0.0016	0.0863 ± 0.0011
a/R_*	12.66 ± 0.77	518 ± 32
ζ/R_* ^c	15.23 ± 0.13	...
R_p/R_*	0.1116 ± 0.0021	...
b^2	$0.209^{+0.054}_{-0.056}$...
$b \equiv a \cos i/R_*$	$0.457^{+0.056}_{-0.066}$...
i (deg)	88.10 ± 0.33	...
Limb-darkening coefficients ^d		
$c_{1,g}$ (linear term)	0.5965	...
$c_{2,g}$ (quadratic term)	0.2045	...
$c_{1,R}$	0.3628	...
$c_{2,R}$	0.3129	...
$c_{1,r}$	0.3896	...
$c_{2,r}$	0.3085	...
$c_{1,i}$	0.2930	...
$c_{2,i}$	0.3208	...
$c_{1,z}$	0.2259	...
$c_{2,z}$	0.3232	...
RV parameters		
K (m s ⁻¹)	92.1 ± 7.8	224 ± 14
e ^e	0.129 ± 0.049	< 0.083
ω	227 ± 29	...
$\sqrt{e} \cos \omega$	-0.233 ± 0.084	...
$\sqrt{e} \sin \omega$	$-0.25^{+0.18}_{-0.11}$...
$e \cos \omega$	-0.082 ± 0.034	...
$e \sin \omega$	-0.090 ± 0.065	...
FEROS RV jitter (m s ⁻¹) ^f ...	< 20.7	...
Coralie RV jitter (m s ⁻¹) ^f ...	58 ± 44	...
PFS RV jitter (m s ⁻¹) ^f	24 ± 14	...
CYCLOPS RV jitter (m s ⁻¹) ^f	93 ± 40	...
Planetary parameters		
M_p (M_J)	0.806 ± 0.069	...
$M_p \sin i$ (M_J)	12.70 ± 0.87
R_p (R_J)	1.126 ± 0.077	...
$C(M_p, R_p)$ ^g	0.05	...
ρ_p (g cm ⁻³)	0.70 ± 0.16	...
$\log g_p$ (cgs)	3.195 ± 0.069	...
a (AU)	0.06112 ± 0.00076	2.504 ± 0.035
T_{eq} (K) ^h	1128 ± 40	175.9 ± 6.4
Θ ⁱ	0.0841 ± 0.0093	...
$\langle F \rangle$ (erg s ⁻¹ cm ⁻²) ⁱ	$(3.66 \pm 0.53) \times 10^8$	$(2.16 \pm 0.32) \times 10^5$

^a For each parameter we give the median value and 68.3% (1σ) confidence intervals from the posterior distribution. Reported results assume an eccentric orbit for HATS-59b and a circular orbit for HATS-59c.

^b Reported times are in Barycentric Julian Date calculated directly from UTC, *without* correction for leap seconds. T_c : Reference epoch of mid transit that minimizes the correlation with the orbital period. Note that HATS-59c has not been observed to transit. We list here the time of mid transit, implied by the orbital solution, in the event that the orbital inclination permits transits. T_{14} : total transit duration, time between first to last contact; $T_{12} = T_{34}$: ingress/egress time, time between first and second, or third and fourth contact. For HATS-59c T_{14} and T_{12} are calculated assuming central transits ($i = 90^\circ$ orbit) and a Jupiter radius for the planet.

^c Reciprocal of the half duration of the transit used as a jump parameter in our MCMC analysis in place of a/R_* . It is related to a/R_* by the expression $\zeta/R_* = a/R_*(2\pi(1 + e \sin \omega))/(P\sqrt{1-b^2}\sqrt{1-e^2})$ (Bakos et al. 2010).

^d Values for a quadratic law, adopted from the tabulations by Claret (2004) according to the spectroscopic (ZASPE) parameters listed in Table 3.

^e For HATS-59c we list the 95% confidence upper-limit on the eccentricity. All other parameters listed are determined assuming a circular orbit for this planet.

^f Error term, either astrophysical or instrumental in origin, added in quadrature to the formal RV errors. This term is varied in the fit independently for each instrument assuming a prior that is inversely proportional to the jitter.

^g Correlation coefficient between the planetary mass M_p and radius R_p determined from the parameter posterior distribution via $C(M_p, R_p) = \langle (M_p - \langle M_p \rangle)(R_p - \langle R_p \rangle) \rangle / (\sigma_{M_p} \sigma_{R_p})$, where $\langle \cdot \rangle$ is the expectation value, and σ_x is the std. dev. of x .

^h Planet equilibrium temperature averaged over the orbit, calculated assuming a Bond albedo of zero, and that flux is reradiated from the full planet surface.

ⁱ The Safronov number is given by $\Theta = \frac{1}{2}(V_{\text{esc}}/V_{\text{orb}})^2 = (a/R_p)(M_p/M_*)$ (see Hansen &

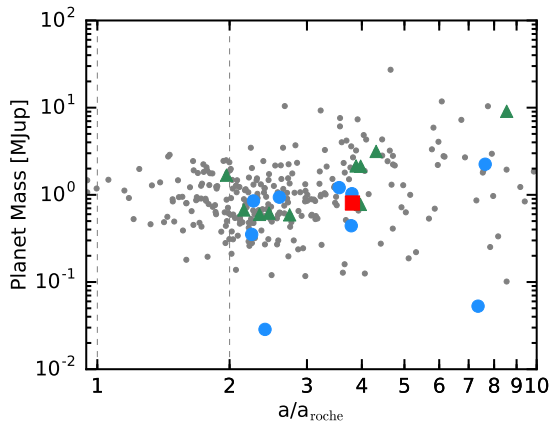


FIG. 8.— Planetary mass vs a/a_{roche} for single (small gray circles), known multi-planetary systems (blue circles), and systems showing a linear trend (green triangles). HATS-59b is shown as a red square. Most of the multi-planetary systems have $a/a_{\text{roche}} > 2$, which supports the high eccentricity migration scenario.

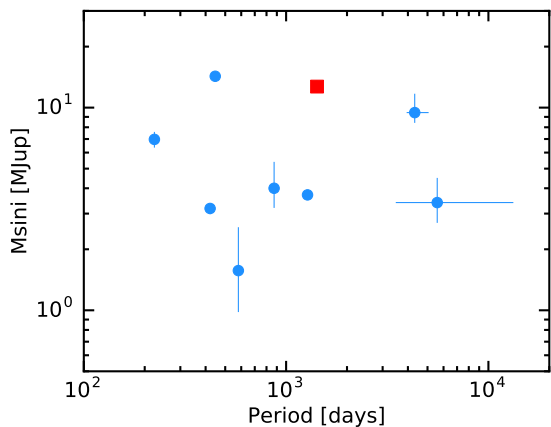


FIG. 9.— $M_{\text{sin}i}$ vs period for the outer companions where the orbit was fully observed (blue circle). HATS-59c (red square) has the third longest period, where only 9 companions have been characterised.

up until they reach the planet-star Roche separation (a_{roche}), the critical distance within which a planet would start losing mass (Faber et al. 2005). On the other hand, high-eccentricity migration predicts planets will circularize at a semimajor axis greater than $2a_{\text{roche}}$. This mechanism would require that hot Jupiters are excited to eccentric orbits, often by being scattered by a distant massive companion, and survived the tidal dissipation process required to circularize their final orbits (Faber et al. 2005; Ford 2006).

Many distant planetary companions to hot Jupiters have been detected (Knutson et al. 2014). In Figure 8 we show planetary mass plotted against a/a_{roche} , where

$$a_{\text{roche}} = 2.7R_p \left(\frac{M_*}{M_p} \right)^{1/3}, \quad (1)$$

for all hot Jupiters whose mass and radii are determined with a precision better than 30% (small gray circles). Blue circles show all the hot Jupiters with a fully resolved orbit of the outer planetary companion and green triangle represent the systems whose RVs show a linear trend, taken from Knutson et al. (2014). The position

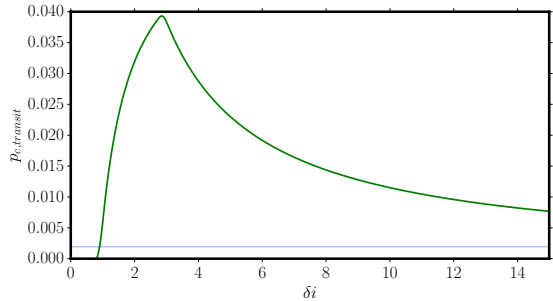


FIG. 10.— Transit probability for HATS-59c for an aligned configuration with HATS-59b as a function of the maximum separation in inclination between both planets. The blue line shows the *a priori* probability for HATS-59c to transit. A maximum probability of $\approx 4\%$ would occur if the orbital plane of HATS-59c is inclined around 3 deg with respect to that of HATS-59b.

TABLE 5
FUTURE TRANSIT
WINDOWS.

Date (UT)	Sun distance (h)
2021-05-30	6.8
2025-04-21	9.4
2029-03-13	12.2

of HATS-59b is shown with a red square. All but one multi-planet system have $a/a_{\text{roche}} > 2$, HAT-P-7b, with a value a/a_{roche} only slightly lower than 2. The available data on hot Jupiters with companions indicate that high eccentricity migration could be the main mechanism for placing the gas giant on a close-in orbit in these systems.

We compare the parameters of HATS-59c to all the detected planetary companions whose orbit is fully resolved. Figure 9 shows the position of HATS-59c (red square) on the minimum mass-period diagram with the other discovered companions (blue circles). With a period of 1422 days, HATS-59c has the third longest period, indicating how few outer companions to transiting hot Jupiters have been characterised due to the lack of RV follow-up observations. All of the companions have minimum masses above $1 M_J$, which is most likely due to selection effects.

4.4. Possible Transits of HATS-59c

As was stated in the previous section, knowing the mutual inclination between HATS-59b and HATS-59c can be useful to further clarify the possible migration path of this system. The host star is too faint for the GAIA mission to be able to measure the astrometric signal of HATS-59c. However, the inclination of HATS-59c with respect to the plane of the sky could be measured if it also transits its star. While the *a priori* probability of transit for HATS-59c is $\sim 0.2\%$, if we consider that the two planets are co-planar, then the probability of transit raises by one order of magnitude. Figure 10 shows the transit probability of HATS-59c for different assumed maximum mutual inclinations (δ_i) between the orbital plane of the planets. The probabilities were computed following the formalism of Beatty & Seager (2010). The maximum probability (3.8%) occurs if the mutual incli-

nation between the planets is around 3 *deg*.

The future transit windows for HATS-59c are listed in Table 5. In this table we indicate the center of the transit window and the distance of the target from the Sun at the time of putative transit center. Currently, the width of the transit window is quite large (> 50 days) due to the large uncertainties in the ephemeris. Long term RV monitoring of the system would be useful to further constrain the width of the transit window.

Acknowledgements— Development of the HAT-South project was funded by NSF MRI grant NSF/AST-0723074, operations have been supported by NASA grants NNX09AB29G, NNX12AH91H, and NNX17AB61G, and follow-up observations receive partial support from grant NSF/AST-1108686. P.S. would like to thank Bertram Bitsch for useful discussions. A.J. acknowledges support from FONDECYT project 1171208, BASAL CATA PFB-06, and project IC120009 “Millennium Institute of Astrophysics (MAS)” of the Millennium Science Initiative, Chilean Ministry of Economy. R.B. acknowledges support from project IC120009 “Millennium Institute of Astrophysics (MAS)” of the Millennium Science Initiative, Chilean Ministry of Economy. L.M. acknowledges support from the Italian Minister of Instruction, University and Research (MIUR) through FFABR 2017 fund. J.H. acknowledges support from NASA grant NNX14AE87G. V.S. acknowledges support from BASAL CATA PFB-06. A.V. is supported by the NSF Graduate Research Fellowship, Grant No. DGE 1144152. This work has made use of data from the European Space Agency (ESA) mission *Gaia* (<https://www.cosmos.esa.int/gaia>), processed by the *Gaia* Data Processing and Analysis Consortium (DPAC, <https://www.cosmos.esa.int/web/gaia/dpac/consortium>). Funding for the DPAC has been provided by national institutions, in particular the institutions participating in the *Gaia* Multilateral Agreement. This work is based on observations made with ESO Telescopes at the La Silla Observatory. This paper also uses observations obtained with facilities of the Las Cumbres Observatory Global Telescope. We acknowledge the use of the AAVSO Photometric All-Sky Survey (APASS), funded by the Robert Martin Ayers Sciences Fund, and the SIMBAD database, operated at CDS, Strasbourg, France. Operations at the MPG 2.2 m Telescope are jointly performed by the Max Planck Gesellschaft and the European Southern Observatory. The imaging system GROND has been built by the high-energy group of MPE in collaboration with the LSW Tautenburg and ESO. We thank the MPG 2.2m telescope support team for their technical assistance during observations.

REFERENCES

- Agol, E., Steffen, J., Sari, R., & Clarkson, W. 2005, *MNRAS*, 359, 567
- Almenara, J. M., Díaz, R. F., Hébrard, G., et al. 2018, *ArXiv e-prints*, a
- Artymowicz, P. 1993, *ApJ*, 419, 166
- Bakos, G. Á., Howard, A. W., Noyes, R. W., et al. 2009, *ApJ*, 707, 446
- Bakos, G. Á., Torres, G., Pál, A., et al. 2010, *ApJ*, 710, 1724
- Bakos, G. Á., Csubry, Z., Penev, K., et al. 2013, *PASP*, 125, 154
- Baruteau, C., Crida, A., Paardekooper, S.-J., et al. 2014, *Protostars and Planets VI*, 667
- Batygin, K., Bodenheimer, P., & Laughlin, G. 2009, *ApJ*, 704, L49
- Bayliss, D., Zhou, G., Penev, K., et al. 2013, *AJ*, 146, 113
- Beatty, T. G., & Seager, S. 2010, *ApJ*, 712, 1433
- Becker, J. C., Vanderburg, A., Adams, F. C., Rappaport, S. A., & Schwengeler, H. M. 2015, *ApJ*, 812, L18
- Brahm, R., Jordán, A., & Espinoza, N. 2017a, *PASP*, 129, 034002
- Brahm, R., Jordán, A., Hartman, J., & Bakos, G. 2017b, *MNRAS*, 467, 971
- Brown, T. M., Baliber, N., Bianco, F. B., et al. 2013, *PASP*, 125, 1031
- Buchhave, L. A., Bakos, G. Á., Hartman, J. D., et al. 2010, *ApJ*, 720, 1118
- . 2011, *ApJ*, 733, 116
- Buhler, P. B., Knutson, H. A., Batygin, K., et al. 2016, *ApJ*, 821, 26
- Butler, R. P., Marcy, G. W., Williams, E., et al. 1996, *PASP*, 108, 500
- Cardelli, J. A., Clayton, G. C., & Mathis, J. S. 1989, *ApJ*, 345, 245
- Claret, A. 2004, *A&A*, 428, 1001
- Crane, J. D., Shtetman, S. A., Butler, R. P., et al. 2010, in *Society of Photo-Optical Instrumentation Engineers (SPIE) Conference Series*, Vol. 7735, *Society of Photo-Optical Instrumentation Engineers (SPIE) Conference Series*
- Dopita, M., Hart, J., McGregor, P., et al. 2007, *Ap&SS*, 310, 255
- Endl, M., Caldwell, D. A., Barclay, T., et al. 2014, *ApJ*, 795, 151
- Espinoza, N., Bayliss, D., Hartman, J. D., et al. 2016, *AJ*, 152, 108
- Faber, J. A., Rasio, F. A., & Willems, B. 2005, *Icarus*, 175, 248
- Ford, E. B. 2006, *ApJ*, 642, 505
- Fortney, J. J., Marley, M. S., & Barnes, J. W. 2007, *ApJ*, 659, 1661
- Goldreich, P., & Tremaine, S. 1980, *ApJ*, 241, 425
- Greiner, J., Bornemann, W., Clemens, C., et al. 2008, *PASP*, 120, 405
- Hansen, B. M. S., & Barman, T. 2007, *ApJ*, 671, 861
- Hardy, R. A., Harrington, J., Hardin, M. R., et al. 2017, *ApJ*, 836, 143
- Hartman, J. D., Bakos, G. Á., Béky, B., et al. 2012, *AJ*, 144, 139
- Hartman, J. D., Bayliss, D., Brahm, R., et al. 2015, *AJ*, 149, 166
- Hellier, C., Anderson, D. R., Collier Cameron, A., et al. 2012, *MNRAS*, 426, 739
- Hippler, S., Bergfors, C., Brandner Wolfgang, et al. 2009, *The Messenger*, 137, 14
- Howard, A. W., Marcy, G. W., Bryson, S. T., et al. 2012, *ApJS*, 201, 15
- Janson, M., Durkan, S., Hippler, S., et al. 2017, *A&A*, 599, A70
- Jin, S., & Mordasini, C. 2018, *ApJ*, 853, 163
- Jordán, A., Brahm, R., Bakos, G. Á., et al. 2014, *AJ*, 148, 29
- Kafer, A., & Pasquini, L. 1998, in *Society of Photo-Optical Instrumentation Engineers (SPIE) Conference Series*, Vol. 3355, *Optical Astronomical Instrumentation*, ed. S. D'Odorico, 844-854
- Knutson, H. A., Fulton, B. J., Montet, B. T., et al. 2014, *ApJ*, 785, 126
- Kovács, G., Bakos, G., & Noyes, R. W. 2005, *MNRAS*, 356, 557
- Kovács, G., Zucker, S., & Mazeh, T. 2002, *A&A*, 391, 369
- Kozai, Y. 1962, *AJ*, 67, 591
- Li, G., Naoz, S., Kocsis, B., & Loeb, A. 2014, *ApJ*, 785, 116
- Lidov, M. L. 1962, *Planet. Space Sci.*, 9, 719
- Lin, D. N. C., Bodenheimer, P., & Richardson, D. C. 1996, *Nature*, 380, 606
- Mancini, L., Lillo-Box, J., Southworth, J., et al. 2016, *A&A*, 590, A112
- Mandel, K., & Agol, E. 2002, *ApJ*, 580, L171
- Mohler-Fischer, M., Mancini, L., Hartman, J. D., et al. 2013, *A&A*, 558, A55
- Mollière, P., & Mordasini, C. 2012, *A&A*, 547, A105
- Mordasini, C., van Boekel, R., Mollière, P., Henning, T., & Benneke, B. 2016, *ApJ*, 832, 41
- Nagasawa, M., Ida, S., & Bessho, T. 2008, *ApJ*, 678, 498
- Neveu-VanMalle, M., Queloz, D., Anderson, D. R., et al. 2016, *A&A*, 586, A93
- Ngo, H., Knutson, H. A., Hinkley, S., et al. 2015, *ApJ*, 800, 138
- Pál, A., Bakos, G. Á., Torres, G., et al. 2008, *ApJ*, 680, 1450
- Penev, K., Bakos, G. Á., Bayliss, D., et al. 2013, *AJ*, 145, 5
- Pepe, F., Ehrenreich, D., & Meyer, M. R. 2014, *Nature*, 513, 358
- Petrovich, C. 2015, *ApJ*, 805, 75
- Queloz, D., Eggenberger, A., Mayor, M., et al. 2000, *A&A*, 359, L13
- Queloz, D., Mayor, M., Udry, S., et al. 2001, *The Messenger*, 105, 1
- Rabus, M., Alonso, R., Belmonte, J. A., et al. 2009, *A&A*, 494, 391
- Schlaufman, K. C. 2018, *ApJ*, 853, 37
- Shporer, A., Zhou, G., Fulton, B. J., et al. 2017, *AJ*, 154, 188
- Sozzetti, A., Torres, G., Charbonneau, D., et al. 2007, *ApJ*, 664, 1190
- Telting, J. H., Avila, G., Buchhave, L., et al. 2014, *Astronomische Nachrichten*, 335, 41
- ter Braak, C. J. F. 2006, *Statistics and Computing*, 16, 239
- Thorngren, D. P., Fortney, J. J., Murray-Clay, R. A., & Lopez, E. D. 2016, *ApJ*, 831, 64
- Triaud, A. H. M. J., Neveu-VanMalle, M., Lendl, M., et al. 2017, *MNRAS*, 467, 1714
- Vogt, S. S., Allen, S. L., Bigelow, B. C., et al. 1994, in *Society of Photo-Optical Instrumentation Engineers (SPIE) Conference Series*, Vol. 2198, *Instrumentation in Astronomy VIII*, ed. D. L. Crawford & E. R. Craine, 362
- Wang, S., Addison, B., Fischer, D. A., et al. 2018, *AJ*, 155, 70
- Weinberg, M. D., Yoon, I., & Katz, N. 2013, *ArXiv e-prints*, 1301.3156
- Winn, J. N., & Fabrycky, D. C. 2015, *ARA&A*, 53, 409
- Yi, S., Demarque, P., Kim, Y.-C., et al. 2001, *ApJS*, 136, 417
- Zhou, G., Bayliss, D., Penev, K., et al. 2014a, *AJ*, 147, 144
- Zhou, G., Bayliss, D., Hartman, J. D., et al. 2014b, *MNRAS*, 437, 2831
- . 2015, *ApJ*, 814, L16